ISSN 0023-1584, Kinetics and Catalysis, 2015, Vol. 56, No. 4, pp. 523–531. © Pleiades Publishing, Ltd., 2015.
Original Russian Text © A.G. Anshits, O.A. Bayukov, N.N. Anshits, O.N. Pletnev, E.V. Rabchevskii, S.N. Vereshchagin, E.V. Kondratenko, 2015, published in Kinetika i Kataliz, 2015, Vol. 56, No. 4, pp. 529–538.

Nature of the Active Sites of Ferrospheres in the Oxidative Condensation of Methane

A. G. Anshits[a, c, *], O. A. Bayukov[b], N. N. Anshits[a], O. N. Pletnev[b], E. V. Rabchevskii[a], S. N. Vereshchagin[a], and E. V. Kondratenko[d]

[a] *Institute of Chemistry and Chemical Technology, Siberian Branch, Russian Academy of Sciences, Krasnoyarsk, 660036 Russia*
[b] *Kirenskii Institute of Physics, Siberian Branch, Russian Academy of Sciences, Krasnoyarsk, 660036 Russia*
[c] *Siberian Federal University, Krasnoyarsk, 660041 Russia*
[d] *Leibniz Institute for Catalysis at the University of Rostock, Rostock, 18059 Germany*
**e-mail: anshits@icct.ru*

Received October 28, 2014

Abstract—The catalytic properties of ferrospheres containing 76–97 wt % Fe_2O_3 in the oxidative condensation of methane were compared with their phase composition and the distribution of iron cations over the crystallographic positions of iron-containing phases in a steady state. It was established that the reaction route of methane oxidation changed at a Fe_2O_3 content of 89 wt %. Deep oxidation was the main reaction route on ferrospheres with a Fe_2O_3 content of <88.8 wt %. At a Fe_2O_3 content of ≥89 wt %, the yield of C_2 hydrocarbons sharply increased and the contribution of deep oxidation decreased. The yield of C_2 hydrocarbons correlated with the amount of defects in the structure of iron spinel, which are iron ions with the tetrahedral cation of Ca^{2+} and the octahedral cation vacancy among the nearest neighbors.

Keywords: oxidative condensation of methane, ferrospheres, iron spinel, Mössbauer spectroscopy, structural defects

DOI: 10.1134/S0023158415040023

INTRODUCTION

The oxidative condensation of methane (OCM) is a promising process for the direct conversion of methane, which is the most inert hydrocarbon constituent of natural gas, into ethylene. The maximum yields of C_2 hydrocarbons can be determined from the known kinetic parameters of the heterogeneous and gas-phase steps of methane oxidation based on the dependence of the selectivity of C_2 hydrocarbon formation (S_{C_2}) on the conversion of methane (X_{CH_4}) [1–3]. In particular, the yield of the C_2 products was no higher than 28% if the process was performed in a CH_4–O_2 mixture [1], and it was 30% under the conditions of a sequential reactant supply [2]. The above theoretical values for C_2 can be considered as bounds for the experiments conducted in a wide range of CH_4/O_2 ratios in the reaction mixture. Zavyalova et al. [3] critically analyzed the results of more than 400 studies published in the last 30 years and found a relationship between the elemental composition and the catalytic properties of different systems in the OCM process at a C_2 yield of 16–30%. With the use of the most effective catalytic systems, in which the yield of the C_2 products was higher than 25%, in fixed-bed flow reactors at temperatures of 943–1223 K, the ratio $CH_4/O_2 = 1.7$–9.0, and contact times of 0.2–5.5 s, S_{C_2} depended on X_{CH_4}. On catalysts with the same elemental composition, the selectivity of the formation of C_2 hydrocarbons monotonically decreased as the conversion of methane increased from 30 to 65%, whereas their yield remained at a level of 25–30%. The experimentally obtained yields of C_2 on the most effective catalytic systems completely correspond to published estimations [1, 2]. The theoretically and experimentally established dependence of S_{C_2} on X_{CH_4} in the heterogeneous–homogeneous OCM process makes it possible to conclude that a highly effective catalyst should not only contain a large quantity of centers for the initiation of $\dot{C}H_3$ radicals but also suppress the surface processes of the deep oxidation of C_1–C_3 hydrocarbons [3].

The problem of finding inexpensive and thermally stable systems that would ensure the required levels of S_{C_2} and methane conversion is of considerable current scientific and practical interest. Among these systems are ferrospheres containing 87.5 wt % Fe_2O_3 and 2.0 wt % MnO with a catalytically active iron spinel phase promoted with calcium, which were isolated from fly ash upon the combustion of high-calcium brown coal [4]. Catalysts on which the conversion of CH_4 at a temperature of 850°C was 24% and the selectivity of the formation of C_2 products was as high as 70% were

obtained by the etching of these ferrospheres with solutions containing HF [5]. At the same time, the narrow fractions of ferrospheres and magnetic cenospheres with a lower iron content exhibited high efficiency as catalysts for the deep oxidation of methane [6, 7].

For determining the reasons for different catalytic actions of ferrospheres in deep oxidation and OCM reactions, we studied the interrelation between the composition, the morphology of globules, the microstructure of iron-containing phases, and the catalytic properties of the narrow fractions of ferrospheres with Fe_2O_3 contents from 36 to 92 wt %, which were separated from the ashes of four known types obtained upon the combustion of coal [8–10]. In particular, it was found that the ferrospheres are formed from melt drops in reducing atmospheres, when iron almost entirely occurs in the state Fe^{2+}. The macrocomponent composition of the test ferrospheres corresponds to the compositions of crystallization range boundaries of primary phases, namely, wustite, fayalite, Fe-cordierite, and hercynite phases, in the state diagram of the $FeO–SiO_2–Al_2O_3$ system [8, 9]. Two main ranges different in the composition and viscosity of the melt from which the ferrospheres are formed can be recognized. At a Fe_2O_3 content to 80 wt %, the behavior of the melt is determined by the properties of the $FeO–SiO_2–Al_2O_3$ system. The ferrospheres of this system are characterized by the presence of alumoferrite spinel, whose concentration increases as the iron content is increased; in this case, the lattice parameter of iron spinel increases from 8.344 to 8.3897 Å. At a Fe_2O_3 content higher than 85%, the behavior of the melt is determined by the FeO–CaO system. Iron spinel promoted with CaO, whose lattice parameter is higher than the corresponding value for stoichiometric magnetite, and a hematite phase with lattice parameters close to the parameters of stoichiometric α-Fe_2O_3 are formed in the ferrospheres of this system [8].

The catalytic properties of the ferrospheres of these two systems in the oxidative methane conversion reaction are also different [10]. The deep oxidation of methane occurs on the ferrospheres that include alumoferrite spinel as an active phase. The deep oxidation reaction is suppressed on the ferrospheres of the FeO–CaO system with an active phase containing calcium ferrite spinel, and the oxidative condensation of CH_4 becomes the main reaction path.

The aim of this work was to study the state and distribution of iron cations over different crystallographic positions of the iron-containing phases of ferrospheres in a steady state and the nature of catalytic centers responsible for the oxidation of methane in different routes using Mössbauer spectroscopy.

EXPERIMENTAL

We examined 11 narrow fractions of high-calcium ferrospheres with an iron oxide content of 76–97%. In this work, the test samples are referred to as B(n), S(n), and SMF(n). The quantity n in parentheses indicates the Fe_2O_3 content of the microspheres (in wt %). The symbols B, S, and SMF designate the source from which the ferrospheres were obtained. The ferrospheres of B(n) and S(n) series were isolated from fly ashes of the FS type formed upon the combustion of coal from the Tugnuisk deposit (Buryatia) and fly ashes of the CS type upon the combustion of coal from the Berezovsky deposit (Krasnoyarsk krai), respectively. A process flowsheet that includes the stages of granulometric classification, magnetic separation, and density separation was used for the isolation of B(n) and S(n) ferrospheres. Sharonova et al. [8] described in detail the separation procedure, the determination of chemical and phase compositions, the morphology of globules, and the microstructural characteristics of the iron-containing phases of the samples of these series. The SMF(n) samples were prepared by the corresponding treatment of samples from the S(n) series. Thus, the SMF(93.51) sample (–0.04+0.032 mm fraction) was obtained by the additional size grading of a fraction of –0.05 mm of the S(89.12) sample with the use of an NSA W/D 200 multifrequency screen analyzer (Technologies, Israel). The SMF(91.36), SMF(96.53), and SMF(97.25) samples with high iron content were obtained by the magnetic separation of a fraction of –0.063+0.05 mm of the S(89.25) sample in a gradient magnetic field with the use of a 138 T magnetic separator (Russia). Table 1 summarizes the chemical composition of all of the test samples.

The catalytic properties of the ferrospheres were studied in a catalytic flow system in fixed-bed quartz microreactors with an inside diameter of 4–8 mm at temperatures of 750–860°C, a reaction mixture of $CH_4 : O_2 : He = 82 : 9 : 9$ (by volume), and a total pressure of 1.3 atm. The ferrosphere sample weight varied from 0.3 to 1.3 g; the catalyst bed length at a maximum load reached 10 mm, and the contact time was 2.24–3.34 s. The composition of the initial mixture and the reaction products was analyzed on an Agilent 7890A GC chromatograph (Agilent, the United States) equipped with HP Plot Al_2O_3 and Molecular Sieve 5A columns and a DB-1 capillary column.

The Mössbauer spectra of the ferrospheres were obtained on an MS-1104Em gamma-resonance spectrometer (Research Institute of Physics of Southern Federal University, Russia) with a Co^{57}(Cr) source at room temperature. For studying the state of iron in the samples after the catalytic experiments, these samples were kept in a flow of the reaction atmosphere for 4 h at 750°C and then rapidly cooled at a rate of 150–200°C/min in the reaction atmosphere.

The interpretation of the spectra was performed in two stages with the use of a modified published procedure [11, 12], according to which the results of Mössbauer spectroscopic studies are interpreted disregarding the complete set of substituent cations in a spinel phase. This circumstance did not allow us to estimate

Table 1. Chemical composition of the narrow fractions of ferrospheres

Sample	Apparent density, g/cm^3	Concentration, wt %								
		SiO_2	Al_2O_3	Fe_2O_3	CaO	MgO	Na_2O	K_2O	TiO_2	SO_3
B(79.12)	1.95	9.00	6.22	79.12	5.40	0.90	0.23	0.08	0.10	0.26
B(76.24)	1.91	9.50	4.64	76.24	9.08	0.81	0.20	0.07	0.19	0.29
B(78.38)	2.07	9.41	5.04	78.38	6.24	1.10	0.20	0.05	0.16	0.24
S(85.20)	1.87	4.00	1.90	85.20	8.69	1.00	0.25	0.07	0.18	0.25
S(88.82)	1.93	2.48	1.20	88.82	7.43	0.81	0.20	0.05	0.19	0.21
S(89.25)	2.57	1.35	1.02	89.25	6.70	0.81	0.24	0.10	0.12	0.28
S(89.12)	2.54	0.64	0.92	89.12	8.81	0.60	0.10	0.05	0.16	0.25
SMF(93.51)	–	1.39	0.19	93.51	3.54	0.40	0.29	0.09	0	0.58
SMF(91.36)	2.69	1.30	0	91.36	6.57	0.33	0.28	0.06	0	0
SMF(96.53)	2.46	0.80	0	96.53	3.20	0.08	0.41	0.04	0	0
SMF(97.25)	2.56	0.36	0	97.25	2.04	0.10	0.28	0.05	0	0

the influence of the cations on the state of the nonequivalent positions of iron and to relate them to the catalytic properties of ferrospheres. In this work, we analyzed experimental data by revealing and identifying the positions of iron, which differ from the appropriate positions in stoichiometric magnetite.

RESULTS AND DISCUSSION

Catalytic Properties of the Ferrospheres

A preliminary study of the catalytic properties of ferrospheres with a Fe_2O_3 content of 36–92 wt % at 600–750°C showed [10] that the dependences of their activity and selectivity for the formation of products on the iron content are complicated and nonmonotonic. In particular, it was found that a sharp increase in the selectivity of the formation of C_2 hydrocarbons was observed at a Fe_2O_3 content higher than 85 wt %. Under the action of a reaction atmosphere, the phase composition and structural parameters of iron-containing phases changed substantially [10].

It is possible to assume that the complex nature of these dependences is determined by the state of iron and the distribution of cations over the crystallographic positions of steady-state phases. In turn, the distribution depends on the macrocomponent composition, process temperature, and reaction mixture composition. In order to eliminate the effect of the oxidation potential of a reaction atmosphere on the distribution of iron cations, catalytic experiments in the course of Mössbauer spectroscopic studies should be carried out at close partial pressures of oxygen. This can be ensured by maintaining close oxygen conversion values in the experiments on different catalytic systems.

The catalytic properties of ferrospheres with a Fe_2O_3 content of 76–97 wt % were studied in a temperature range of 750–860°C. At a Fe_2O_3 content of 89 wt %, a sharp increase in the yield of C_2 was observed in the entire temperature range, and this yield noticeably decreased as the iron content was further increased (Fig. 1). The observed dependences of the yield of methane oxidation products on the Fe_2O_3 content are indicative of a change in the reaction route on going to the ferrospheres with a Fe_2O_3 content of ≥ 89 wt %. On these samples, the maximum value of S_{C_2} = 62–72% was attained at 825°C and an oxygen conversion of no higher than 85%. At the same time, the selectivity for C_2 formation on the ferrospheres of B and S series with a Fe_2O_3 content of ≤ 89 wt % was 10–20% at a 100% conversion of oxygen. A constant level of the yield of CO_2 on these samples is explained by the complete conversion of oxygen. The yield of CO remained at a low level of no higher than 0.8% over the entire range of iron concentrations (Fig. 1).

As the temperature was increased to 850°C, the maximum yield of C_2 (8.2%) was reached on the SMF(91.36) sample and shifted toward higher iron content. Note that the yields observed at high temperatures were almost coincident with the corresponding values obtained on high-calcium ferrospheres, which include $(Ca,Fe)Fe_2O_4$ as an active phase with the unit cell parameter a_0 = 8.405 Å [4]. A somewhat higher C_2 yield of ~13% at 825°C was observed with the use of single-phase $ZnFe_2O_4$ spinel with a_0 = 8.442 Å as a catalyst [13]. In this case, S_{C_2} was no higher than 65%.

At 750°C, the high degrees of oxygen conversion X_{O_2} = 95, 100, and 77% were obtained only on the three catalysts B(76.2), B(78.4), and B(79.1), respectively. On the samples of S and SMF series with a Fe_2O_3 content of ≥ 85.2 wt %, the concentration of oxygen changed insignificantly upon passing through the reactor; the conversion X_{O_2} varied from 9 to 27%, which corresponds to a partial oxygen pressure of 0.095–0.085 atm at the reactor outlet under steady-

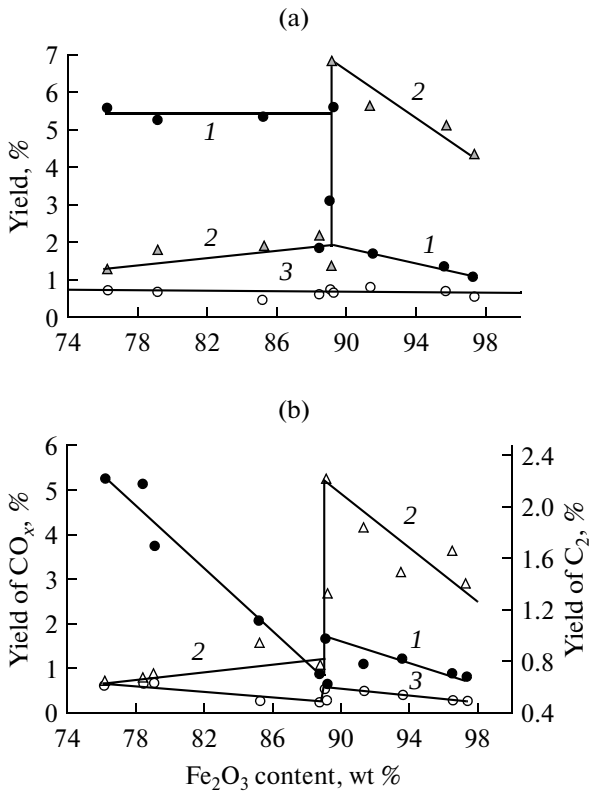

Fig. 1. Dependence of the yield of methane oxidation products on the total iron content of ferrospheres at temperatures of (a) 825 and (b) 750°C: (*1*) CO_2, (*2*) C_2, and (*3*) CO.

state conditions. An insignificant change in the concentration and close degrees of oxygen conversion allowed us to assume that the formation of a redox steady state in the major portion of ferrosphere samples occurred at similar partial pressures of O_2. Therefore, the catalysts after the catalytic experiments performed on them at 750°C were used for studying the effect of the distribution of iron cations on the yields of OCM products.

For the samples with a Fe_2O_3 concentration of <89 wt %, CO_2 was the main reaction product at 750°C, and its yield dramatically decreased as the Fe_2O_3 content was increased from 76.2 to 88.8 wt %. For the S(88.8) sample, the yields of CO_2 and C_2 were approximately the same (0.75–0.8%). For the ferrospheres with a Fe_2O_3 content of 89–97 wt % C_2 hydrocarbons became the main product, whose yield sharply increased to 2.2% and then monotonically lowered as the concentration of Fe_2O_3 was increased. Analogous dependence, although with a smaller amplitude, was observed for CO_2 (Fig. 1b). These differences can be related to the state and the distribution of iron cations over the crystallographic positions of phases in a steady state of the ferrospheres formed from the melts of two different systems: $FeO–SiO_2–Al_2O_3$ and FeO–CaO.

State and Distribution of Iron Cations in Ferrospheres in the Initial and Steady States

The state and distribution of iron over the phases and crystallographic positions were studied by the Mössbauer spectroscopy of ferrospheres in the initial and steady states after catalytic experiments performed on them at 750°C. As an example, Table 2 summarizes the parameters of the spectra of ferrospheres with strongly different catalytic properties.

In accordance with X-ray structural analysis [8], the following three main iron-containing phases are present in ferrospheres in the initial and steady states: magnetite, hematite, and aluminosilicate glass. Hematite is identified based on the parameters characteristic of a sextet ($IS \approx 0.38$ mm/s, $H \approx 517$ kOe, and $QS \approx -0.38$ mm/s) in the Mössbauer spectra [14], and magnetite is identified based on the presence of $Fe^{2.5+}$ iron positions with rapid electron exchange [15]. The enormous width of the lines of quadrupole doublets suggests a large set of positions with different degrees of distortion, which is characteristic of an amorphous or glassy state of substance. Therefore, the paramagnetic parts of the spectrum were assigned to the iron that occurred in aluminosilicate glass.

The spinel phase of all of the samples was defect diamagnetically diluted magnetite (Table 2). Two sextets are usually present in the spectrum of stoichiometric magnetite above the Verwey transition point (~125 K, the temperature of the transition of cubic Fe_3O_4 into a structure with lower symmetry). The first is caused by the presence of trivalent iron cations that occupy tetrahedral positions Fe^{3+} (A), and the second, by the presence of $Fe^{2.5+}$ (B) cations in an octahedral environment. The parameters of these positions are the following: $IS = 0.3$ mm/s and $H = 490$ kOe for Fe^{3+} (A); $IS = 0.66$ mm/s and $H = 460$ kOe for $Fe^{2.5+}$ (B). In the first approximation, two sextets are observed below the Verwey temperature: Fe^{3+} (A + B) and Fe^{2+} (B) [16]. The spectra of the positions Fe^{3+} (A) and Fe^{3+} (B) are unresolved. The positions A and B in maghemite γ-Fe_2O_3 are also unresolved [17]. On this basis, we believe that the positions in the ferrospheres designated as Fe^{3+} (A + B) and $Fe^{2.5+}$ (B) in Table 2 analogous to the positions of stoichiometric magnetite.

In the stoichiometric magnetite $Fe_3O_4 \equiv (Fe^{3+})[Fe^{2+}Fe^{3+}]O_4 \equiv (Fe^{3+})[Fe_2^{2.5+}]O_4$, the ratio of the number of Fe^{2+} cations to the total number of iron atoms is 0.333. In the spinel phase of ferrospheres, the above ratio is considerably lower (Fig. 2), and it strongly changes depending on the iron content of the ferrospheres. This deviation is caused by the defectiveness of magnetite, which can result form the replacement of iron cations by diamagnetic cations and cation and anionic vacancies and associated spinel lattice distortions. In particular, experimental results [18–20] evidenced that the Ca^{2+} cations in magnetite are located in the tetrahedral positions. At low spinel doping lev-

Table 2. Mössbauer parameters of ferrospheres in the initial and steady states

Fraction	Initial state					Steady state at 750°C					Position
	$IS \pm 0.005$, mm/s	$H \pm 3$, kOe	$QS \pm 0.02$, mm/s	$W \pm 0.02$, mm/s	$A \pm 0.03$	$IS \pm 0.005$, mm/s	$H \pm 3$, kOe	$QS \pm 0.02$, mm/s	$W \pm 0.02$, mm/s	$A \pm 0.03$	
B(79.12)	0.406	505	–0.06	0.43	0.14	0.379	517	–0.36	0.35	0.30	α-Fe_2O_3
	0.303	489	0.10	0.41	0.30	0.278	493	0.08	0.53	0.22	Fe^{3+} (A + B)
	0.447	468	–0.21	0.61	0.20	0.434	473	–0.35	0.74	0.22	Fe^{v3+} (B)
	0.667	459	–0.01	0.35	0.07	0.648	456	0	0.47	0.12	$Fe^{2.5+}$ (B)
	0.721	435	–0.01	0.87	0.22	0.628	423	–0.29	0.83	0.09	$Fe^{v2.5+}$ (B)
	0.567	–	–	2.32	0.07	0.181	–	–	2.19	0.04	PM (Fe^{3+})
S(88.82)	0.318	518	–0.30	0.25	0.22	0.378	517	–0.32	0.40	0.58	α-Fe_2O_3
	0.220	492	0	0.32	0.31	0.280	496	0.06	0.54	0.15	Fe^{3+} (A + B)
	0.599	461	–0.03	0.40	0.39	0.664	459	0	0.56	0.14	$Fe^{2.5+}$ (B)
	0.368	415	0.20	0.69	0.06	0.337	397	0.85	0.92	0.05	Fe^{vv3+} (B)
	0.223	–	0.88	0.65	0.03	0.208	–	–	3.83	0.09	PM (Fe^{3+})
S(89.12)	0.382	517	–0.32	0.24	0.38	0.379	521	–0.32	0.39	0.51	a-Fe_2O_3
	0.311	491	0	0.44	0.28	0.298	503	0	0.53	0.14	Fe^{3+} (A + B)
	0.653	457	0.01	0.50	0.18	0.685	459	–0.02	0.54	0.08	$Fe^{2.5+}$ (B)
	0.460	402	0.36	1.12	0.11	0.238	389	0.37	1.52	0.15	Fe^{vv3+} (B)
	0.272	–	0.88	0.78	0.05	0.158	–	–	3.01	0.12	PM (Fe^{3+})
S(96.53)	0.318	519	–0.30	0.25	0.36	0.366	523	–0.28	0.29	0.64	α-Fe_2O_3
	0.226	491	0.05	0.36	0.24	0.295	495	0	0.27	0.08	Fe^{v3+} (B)
	0.612	461	0.06	0.43	0.22	0.640	463	0.01	0.40	0.14	$Fe^{2.5+}$ (B)
	0.576	417	–0.02	0.53	0.04	–	–	–	–	–	$Fe^{v2.5+}$ (B)
	0.271	387	0.58	0.60	0.04	0.322	402	0.76	0.71	0.08	Fe^{vv3+} (B)
	0.315	–	1.70	1.48	0.09	0.286	–	1.18	1.33	0.06	PM (Fe^{3+})

IS is the isomeric chemical shift relative to α-Fe; *H* is the hyperfine magnetic field on Fe nuclei; *QS* is the quadrupole splitting; *W* is the absorption line width; and *A* is the population of Fe positions.

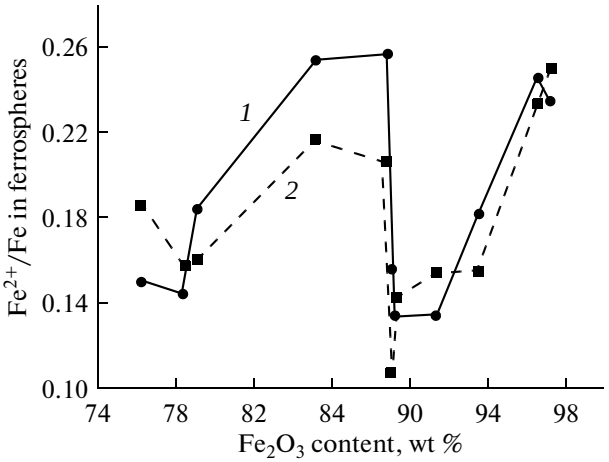

Fig. 2. Dependence of the Fe^{2+} content of the spinel phase on the total iron content of the ferrospheres in the (*1*) initial and (*2*) steady states.

els, the cations Al^{3+} and Ti^{4+} are arranged in the octahedral positions. The cations Mg^{2+} occupy the positions of both types, preferably, octahedral [21].

Along with the positions corresponding to stoichiometric magnetite, the test ferrospheres had additional positions, which are designated as Fe^{v3+}, $Fe^{v2.5+}$, and Fe^{vv3+}. Table 3 summarizes the characteristics of the positions of iron detected in a spinel phase. Figure 3 shows the fragments of a spinel structure to elucidate the appearance of nonequivalent positions in defect magnetite. The positions of iron in the spinel phase of ferrospheres are designated as cations in a specific charge state.

Tetrahedral cation A has 12 nearest octahedral neighbors; therefore, insignificant diamagnetic dilution in the octahedral sublattice with the rupture of one of 12 magnetic couplings does not exert a substantial influence on the hyperfine fields on the iron nuclei of sublattice sites. Octahedral cation B has only six tetrahedral neighbors, and the replacement of one cation A by a diamagnetic cation weakens the hyperfine field on cation B by 15–20 kOe due to a decrease in the number of magnetic couplings [22–24]. The position of Fe^{v3+}(B), which is characterized by the presence of a hyperfine field of ~470 kOe, appears upon the appearance of the diamagnetic cation Ca^{2+} or Mg^{2+} among the nearest neighbors A. The charge reduction $Fe^{3+} \rightarrow Ca^{2+}$ in the tetrahedral sublattice creates electron deficiency on the nearest oxygen atom, and the condition of electroneutrality requires an increase in the charge in the octahedral sublattice $Fe^{2.5+}$ (B) $\rightarrow$ Fe^{v3+} (B). The loss of one magnetic coupling of an octahedral cation with tetrahedral cations weakens a hyperfine field from 495 kOe (Fe^{3+} (A + B)) for stoichiometric magnetite (Fig. 3a) to 470 kOe for Fe^{v3+} (B) (Table 3, Fig. 3b).

Upon the appearance of the nearest diamagnetic cation A, the $Fe^{2.5+}$ positions of stoichiometric magnetite are converted into the $Fe^{v2.5+}$ positions. As a result of the loss of a magnetic coupling with the tetrahedral sublattice, a hyperfine field is weakened from 460 to 426 kOe (Table 3).

The occurrence of the Ca^{2+} cation, which possesses a large ionic radius (1.04 Å), in small tetrahedral positions provokes the appearance of a cation vacancy near it; because of this, local distortions and a charge gradient across the lattice appear. Therefore, the appearance of the Fe^{vv3+} (B) position with $H = 400$ kOe can be explained by the presence of two defects: tetrahedral Ca^{2+} (A) and a cation vacancy among the neighbors of cation B (Fig. 3c). It is clear that these positions are a consequence of the transformation of the $Fe^{2.5+}$ (B) positions of stoichiometric magnetite, and they do not participate in the process of rapid electron exchange on the localization of an electron of the cation on the oxygen atom.

With consideration for all of the detected states, a decrease in the concentration of iron spinel and an increase in the contribution of a hematite phase were observed in the initial samples as the total Fe_2O_3 content was increased (Fig. 4a). After conducting the catalytic experiments (Fig. 4b), the hematite content increased and the iron spinel content decreased, and this effect manifested itself to the greatest degree on catalysts with a high concentration of Fe_2O_3. The con-

Table 3. Positions of iron in the spinel phase of ferrospheres identified by Mössbauer spectroscopy

Iron position	*IS*, mm/s	*H*, kOe	Local environment of the position
Fe^{3+} (A + B)	0.27 ± 0.04	495 ± 6	Stoichiometric magnetite
$Fe^{2.5+}$ (B)	0.64 ± 0.04	460 ± 3	Stoichiometric magnetite, rapid electron exchange
Fe^{v3+} (B)	0.43 ± 0.04	470 ± 3	Diamagnetic A^{2+} neighbor, electron localization on oxygen
$Fe^{v2.5+}$ (B)	0.65 ± 0.07	426 ± 8	Diamagnetic A^{2+} neighbor, rapid electron exchange
Fe^{vv3+} (B)	0.37 ± 0.13	400 ± 20	Ca^{2+} (A) neighbor + cation vacancy, electron localization on oxygen

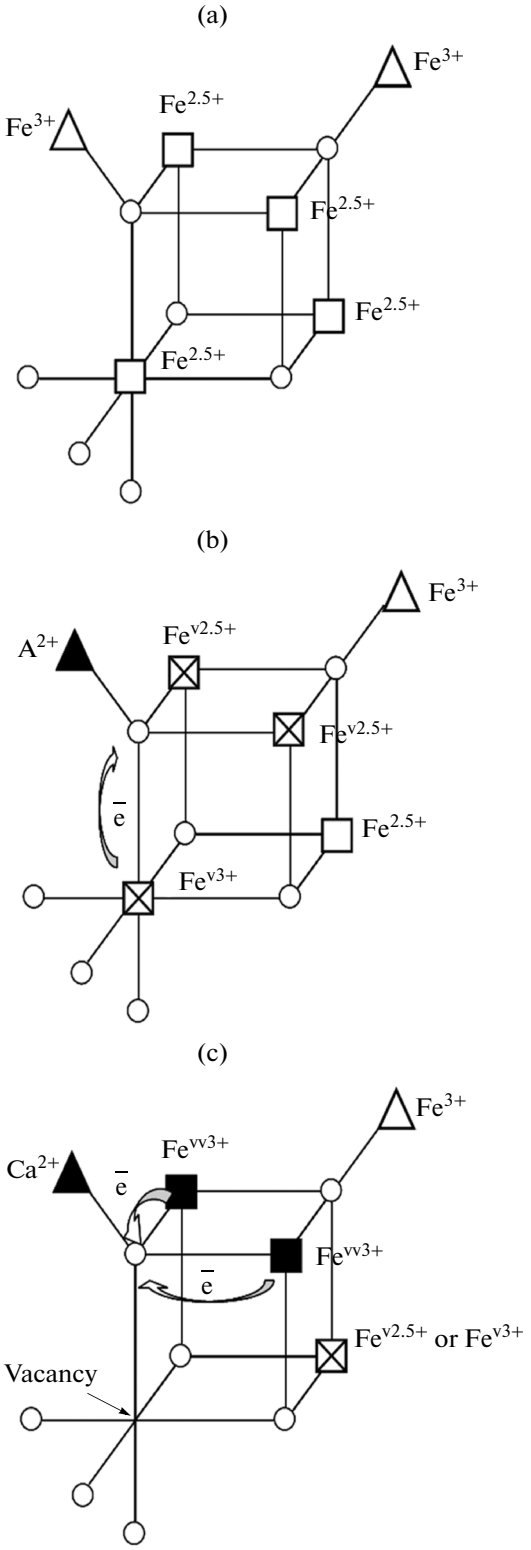

Fig. 3. Spinel structure fragments: (a) the position of iron in stoichiometric magnetite, (b) A^{2+}-substituted magnetite, and (c) Ca^{2+}-substituted magnetite with a cation vacancy. Notation: (○) oxygen, (□) octahedral cations, and (▲) tetrahedral cations.

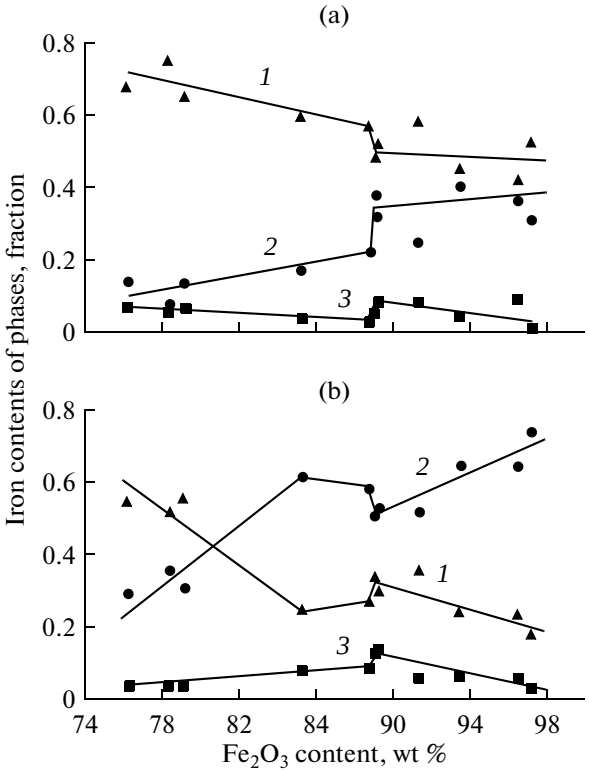

Fig. 4. Dependence of the iron content of (*1*) iron spinel, (*2*) hematite, and (*3*) an amorphous phase in the (a) initial and (b) steady states on the total iron concentration in the ferrospheres.

centration of an amorphous phase in a steady state varied from 3 to 13% with a pronounced maximum at a Fe_2O_3 concentration of 89 wt %.

Nature of the Active Sites of the Oxidative Conversion of Methane

Oxide systems with the structure of spinel AB_2O_4 are effective catalysts for the deep oxidation of methane in an excess of oxygen. The comparison of the specific catalytic activities of the binary oxides with a spinel structure (chromites [25], cobaltites [25, 26], and ferrites [27, 28]) and 3*d*-metal oxides in the oxidation reactions of hydrogen and methane showed that the cations that are the constituents of spinel do not manifest the additivity property. Trivalent cations in an octahedral coordination play the main role, and bivalent cations in a tetrahedral environment are of secondary importance. The activity of these systems depends on the binding energy of oxygen, which primarily depends on the cations Cr^{3+}, Co^{3+}, and Fe^{3+} in the octahedral position of spinel. The strongest bond is Fe^{3+}–O. Therefore, of the above oxide systems with the structure of spinel, ferrites manifest the smallest activity [25, 29]. It was found that their activity in the reaction of methane oxidation at 425°C changes approximately by an order of magnitude (from 28.7 ×

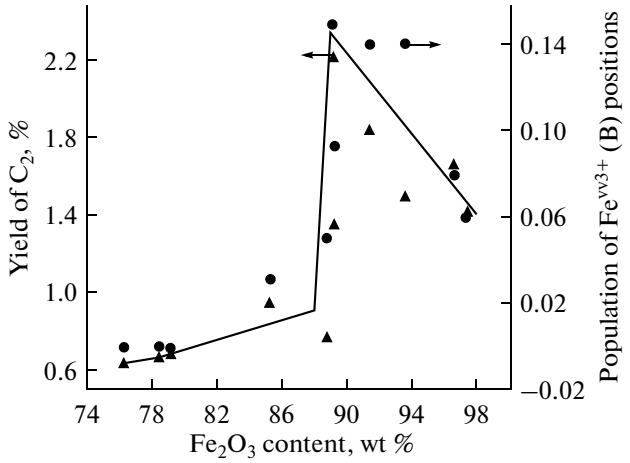

Fig. 5. Dependence of (▲) the yield of C_2 products and (●) the population of Fe^{vv3+} (B) positions in a steady state on the total iron content of the ferrospheres.

10^{11} to 3.4×10^{11} (O_2 molecule) $cm^{-2}\ s^{-1}$) in the order $NiFe_2O_4 > CoFe_2O_4 > CdFe_2O_4 > CuFe_2O_4 > ZnFe_2O_4 > MgFe_2O_4 > MnFe_2O_4$, and they are much inferior to Fe_2O_3 in activity (52×10^{11} (O_2 molecule) $cm^{-2}\ s^{-1}$) [27]. The published data cited indicate that the low yields of CO_2 on the samples with a Fe_2O_3 content of ≥89 wt % (Fig. 1) cannot be explained by a high concentration of the α-Fe_2O_3 phase in a steady state (Fig. 4b).

It is important to note the symbatic dependences of the yield of CO_2 (Fig. 1b) and the concentration of the spinel phase of ferrospheres in a steady state (Fig. 4b). Therefore, it is possible to assume that the activity of ferrospheres in the deep oxidation reaction of methane depends, according to published data [25, 29], on the binding energy of lattice oxygen in the spinel phase of ferrospheres.

Note that the $Fe^{vv3+т}$(B) positions were detected only in the high-iron ferrospheres from S and SMF series. In this case, their content in the ferrospheres with a total Fe_2O_3 concentration of ≥89 wt % considerably increased (Table 2). By this is meant that the Fe^{vv3+} (B) positions can participate in the stabilization of the oxygen forms that are active in the OCM process.

As noted above, the activity of ferrospheres in the deep oxidation of methane is determined by the bonding energy of lattice oxygen in the iron spinel phase. In contrast to this, oxygen species stabilized on the structural defects of the catalyst participate in the OCM process. Different aspects of the effect of structural defects on the catalytic properties of single-phase and polyphase oxide systems in the OCM process have been widely discussed in the literature [30–36]. The role of the impurity and intrinsic structural defects of unreducible, reducible, simple, and multicomponent oxide systems in the formation of active oxygen species in CH_4–O_2 and CH_4–N_2O reaction atmospheres was considered in detail in a survey [32]. The participation of the active surface oxygen species O^- is assumed for the majority of oxide systems effective in the OCM reaction from different structural types [30–35]. The mechanism of the formation of this species depends on the defect centers present in the system. For example, Yan et al. [35] used Mössbauer spectroscopy to demonstrate a relationship between the yield of C_2 and the concentration of Fe^{4+} ions in the iron-containing catalysts $Ca(Sr,Ba)_{0.5}La_{1.5}Fe_{0.5}Li_{0.5}O_4$ and $SrLaFe_{0.5}Zn(Mg)_{0.5}O_4$ with the structure of K_2NiF_4. According to Yan et al. [35], the O^- species, which is active in the OCM reaction, is formed according to the reaction scheme

$$Fe^{4+} + O^{2-} = Fe^{3+} + O^-.$$

On the three catalysts $Ca(Sr,Ba)LaFeLiO_4$ with a high Fe^{4+} content, a high yield of C_2 was observed; at 800°C and the mixture of $CH_4 : O_2 = 2 : 1$, this yield was 22% at $S_{C_2} = 54$–57%. The replacement of the iron ion by zinc or magnesium ions in the $SrLaFe_{0.5}Zn(Mg)_{0.5}O_4$ system increased the Fe^{4+} content and the yield of C_2. This replacement led to the conversion of 50% Fe^{3+} ions into Fe^{4+} and to an increase in the yield of C_2 by a factor of more than 2 to 14–15%.

Unlike the $SrLaFe_{0.5}Zn(Mg)_{0.5}O_4$ system, where the replacement of Fe^{3+} by Zn^{2+} and Mg^{2+} ions causes the formation of Fe^{4+}, the occurrence of Ca^{2+} in the tetrahedral positions of spinel leads to the formation of the Fe^{vv3+} defect state in the high-iron ferrospheres. Figure 5 shows the dependence of the fraction of these positions in a steady state of ferrospheres and the yield of C_2 on the same samples on the total iron concentration in them. The same character of these two dependences, including a sharp increase in both of the quantities at a Fe_2O_3 content of 89 wt % is indicative of the participation of Fe^{vv3+} (B) in the stabilization of the oxygen species that is active in the OCM process.

Strictly speaking, the Ca^{2+}-substituted fragment of a spinel structure should be considered as an active center (Fig. 3c). It was demonstrated above that the inclusion of the Ca^{2+} ion facilitates the formation of a cation vacancy. As a result, the oxygen of a spinel phase near these defects experiences considerable electron deficiency, which is made up by the presence of the adjacent iron cations. The resulting pair of $Fe^{vv3} + O^{2-}_{def}$ increases the Madelung energy of the lattice because of the appearance of a charge gradient, and it tends to return into the ground state when occasion offers. In ordinary iron oxide compounds, the ligand–cation electron excitation energy is 4–8 eV [37]. This energy is considerably lower for the $Fe^{vv3} + O^{2-}_{def}$ state.

We assume that the interaction of methane with oxygen [$Fe^{vv3} + O^{2-}_{def}$] is a one-electron process, which ensures the formation of $\dot{C}H_3$ radicals whose recombination in a gas phase affords ethane. The oxidation surface OH groups leads to the release of H_2O and the regeneration of the active center.

CONCLUSIONS

Thus, in this work, we compared the catalytic properties of ferrospheres containing 76–97 wt % Fe_2O_3 in the oxidation reaction of methane with the state and the distribution of iron cations over the crystallographic positions of iron-containing phases in a steady state. The ferrospheres included iron spinel and hematite as the main phases. In the steady state, the concentrations of a hematite phase and spinel increased and decreased, respectively, as the total iron concentration was increased. The symbatic dependences of the yield of CO_2 and the spinel phase content on the total iron concentration in the ferrospheres indicated the participation of the lattice oxygen of iron spinel in the deep oxidation of methane.

The spinel phase is defective magnetite. In the low-iron ferrospheres, it is diluted with the diamagnetic cations of Al and Mg. In the spinel phase of the high-iron microspheres, the positions of iron with the tetrahedral Ca^{2+} cation and the octahedral cation vacancy were detected among the nearest neighbors. The concentration of these structural defects correlates with the yield of C_2 hydrocarbons. The oxygen ion of a spinel phase near these defects acts as an active oxygen species in the OCM reaction.

ACKNOWLEDGMENTS

This work was supported by the Russian Science Foundation (grant no. 14-13-00289).

REFERENCES

1. Su, Y.S., Ying, J.Y., and Green, W.H., *J. Catal.*, 2003, vol. 218, p. 321.
2. Labinger, J.A., *Catal. Lett.*, 1988, vol. 1, p. 371.
3. Zavyalova, U., Holena, M., Schlögl, R., and Baerns, M., *ChemCatChem*, 2011, vol. 3, p. 1835.
4. Anshits, A.G., Voskresenskaya, E.N., Kondratenko, E.V., Fomenko, E.V., and Sokol. E.V., *Catal. Today*, 1998, vol. 42, p. 197.
5. Fomenko, E.V., Kondratenko, E.V., Sharonova, O.M., Plekhanov, V.P., Koshcheev, S.V., Boronin, A.I., Salanov, A.N., Bajukov, O.A., and Anshits, A.G., *Catal. Today*, 1998, vol. 42, p. 273.
6. Anshits, A.G., Kondratenko, E.V., Fomenko, E.V., Kovalev, A.M., Bajukov, O.A., Anshits, N.N., Sokol, E.V., Kochubey, D.I., Boronin, A.I., Salanov, A.N., and Koshcheev, S.V., *J. Mol. Catal. A: Chem.*, 2000, vol. 158, p. 209.
7. Anshits, A.G., Kondratenko, E.V., Fomenko, E.V., Kovalev, A.M., Anshits, N.N., Bajukov, O.A., and Sokol, E.V., *Catal. Today*, 2001, vol. 64, p. 59.
8. Sharonova, O.M., Anshits, N.N., Solovyov, L.A., Salanov, A.N., and Anshits, A.G., *Fuel*, 2013, vol. 111, p. 332.
9. Sharonova, O.M., Anshits, N.N., and Anshits, A.G., *Inorg. Mater.*, 2013, vol. 49, p. 586.
10. Vereshchagin, S.N., Kondratenko, E.V., Rabchevskii, E.V., Anshits, N.N., Solovyov, L.A., and Anshits, A.G., *Kinet. Catal.*, 2012, vol. 53, no. 4, p. 449.
11. Anshits, N.N., Bajukov, O.A., Eremin, E.V., Solovyov, L.A., Rabchevskii, E.V., and Anshits, A.G., *Phys. Solid State*, 2010, vol. 52, p. 1188.
12. Bajukov, O.A., Anshits, N.N., Petrov, M.I., Balaev, A.D., and Anshits, A.G., *Mater. Chem. Phys.*, 2009, vol. 114, p. 495.
13. Papa, F., Patron, L., Carp, O., Paraschiv, C., and Ion, B., *J. Mol. Catal. A: Chem.*, 2009, vol. 299, p. 93.
14. Kundig, W. and Bommel, H., *Phys. Rev.*, 1966, vol. 142, p. 327.
15. Daniels, J.M. and Rosencwaig, A., *J. Phys. Chem. Solids*, 1969, vol. 30, p. 1561.
16. Ito, A., Ono, K., and Ishikawa, Y., *J. Phys. Soc. Jpn.*, 1963, vol. 18, p. 1465.
17. Armstrong, R.J., Morrish, A.H., and Sawatzky, G.A., *Phys. Lett. A.*, 1966, vol. 23, p. 414.
18. De Sitter, J., Govaert, A., De Grave, E., Chambaere, D., and Robbrecht, G., *Phys. Status Solidi A*, 1977, vol. 43, p. 619.
19. Gerardin, R., Banazebi, A., Millon, E., Brice, J.F., Evrard, O., and Sandez, J.P., *J. Solid State Chem.*, 1989, vol. 78, p. 154.
20. Cieslak, J., Dubiel, S.M., Orewczyk, J., and Jasienška, S., *J. Phys. IV*, 1997, vol. 07, p. C1_589.
21. Krupička, C., *Physik der Ferrite und der verwandten magnetischen Oxide*, Prague: Academia, 1973.
22. Sawatzky, G.A., van der Woude, F., and Morrish, A.H., *Phys. Rev.*, 1969, vol. 187, p. 747.
23. Petir, G.A. and Forester, D.W., *Phys. Rev.*, vol. 4, p. 3912.
24. Bashkirov, Sh.Sh., Liberman, A.B., and Sinyavskii, V.I., *Fiz. Tverd. Tela*, 1972, vol. 14, p. 3264.
25. Boreskov, G.K., Popovskii, V.V., and Sazonov, V.A., *Trudy IV mezhd. Kongr. po katalizu* (Proc. IV Int. Congr. on Catalysis), Moscow, 1970, vol. 1, p. 343.
26. Andrushkevich, T.V., Boreskov, G.K., Popovskii, V.V., Muzykantov, V.S., Kimkhai, O.N., and Sazonov, V.A., *Kinet. Katal.*, 1968, vol. 9, no. 3, p. 595.
27. Boreskov, G.K., Popovskii, V.V., Lebedeva, N.E., Sazonov, V.A., and Andrushkevich, T.V., *Kinet. Katal.*, 1970, vol. 11, no. 5, p. 1253.
28. Popovskii, V.V., Boreskov, G.K., Dzevenski, Z., Muzykantov, V.S., and Shul'meister, T.T., *Kinet. Katal.*, 1971, vol. 12, no. 4, p. 979.
29. Boreskov, G.K., Kataliz: *Voprosy teorii i praktiki* (Catalysis: Topics in Theory and Practice), Novosibirsk: Nauka, 1987.
30. Lansford, J.H., *Catal. Today*, 1990, vol. 6, p. 235.
31. Zhang, Z., Verykios, X.E., and Baerns, M., *Catal. Rev. Sci. Eng.*, 1994, vol. 36, p. 507.
32. Voskresenskaya, E.N., Roguleva, V.G., and Anshits, A.G., *Catal. Rev. Sci. Eng.*, 1995, vol. 37, p. 101.
33. Maksimov, N.G., Selyutin, G.E., Anshits, A.G., Kondratenko, E.V., and Roguleva, V.G., *Catal. Today*, 1998, vol. 42, p. 279.
34. Kondratenko, E.V. and Baerns, M., *Handbook of Heterogeneous Catalysis*, Weinheim: Wiley-VCH, 2008, vol. 8, p. 3010.
35. Yan, Q., Jin, Y., Wang, Y., Chen, Y., and Fu, X., *Proc. 10th Int. Congr. on Catalysis*, Budapest, 1992, p. 2230.
36. Burrows, A., Kiely, Ch.J., Hutchings, G.J., Joyner, R.W., and Sinev, M.Yu., *J. Catal.*, 1997, vol. 167, p. 77.
37. Bayukov O.A. and Savitskii, A.F., *Phys. Solid State*, 1994, vol. 36, p. 1049.

Translated by V. Makhlyarchuk